Hybrid Solar Thermal Power Plants

Jorge Augusto Maciel Milhomem Rodrigues
jorgemilhomem@tecnico.ulisboa.pt

Instituto Superior Técnico, Universidade de Lisboa, Portugal

June 2019

Abstract

Solar thermal energy, especially concentrated solar power (CSP), represents an increasingly attractive renewable energy source. One of the key factors that determines the development of this technology is its integration with efficient power cycles. So, as to make CSP an attractive alternative to the conventional thermodynamic cycles present in most of today's thermal power plants, it is of high relevance to develop models that provide attractive global efficiencies and cost effective CO_2 mitigation. The present work focuses on the energetic study of three combined Brayton-Rankine cycles hereby proposed, in which features as having a combustion chamber in series with a solar receiver, and a stream splitter subsequent to the gas turbine were studied and compared. The main source of heat is provided by parabolic trough collectors. The thermodynamic analyses are performed for selected working fluids including CO_2, air, N_2, He and H_2 for the topping cycles, and R-245fa, R-141B, Cyclohexane, n-Pentane, and Water for the bottoming cycle, resulting in 25 fluid combinations. A MATLAB program was developed to perform the simulations. The results show that the CO_2 and R-245fa fluid pair provides the highest cycle efficiency curves. In addition, stream splitting proves to be advantageous, compared to other layouts found in literature.
Keywords: Concentrated solar power, thermodynamics, hybrid power cycles.

1. Introduction

Climate change and global warming are major concerns in the present days. The increasing world population, accompanied by the growth of energy demand makes the development of sustainable and clean energy technologies of primary importance in order to reduce emissions of carbon dioxide and other greenhouse gases.

Solar energy is being seen more and more as a promising energy source to achieve better results in both the environmental and financial aspects. A promising technology is concentrated solar power (CSP), which often offers the most reliable and dispatchable power generation from sun irradiation [7]. CSP technologies make use of the entire solar irradiation spectrum by using mirrors or lenses to concentrate the sun's rays, providing a source of heat to generate electricity. Thus, CSP technologies are an alternative to fossil fuels or nuclear reactions regarding energy production. Four major CSP technologies are implemented around the globe [8, 10]: Parabolic Trough Collectors (PTC); Linear Fresnel Collectors (LFC); Solar Power Towers (SPT); Parabolic Dish Collectors (PDC).

In order to generate electricity, the concentrated irradiation is converted to heat, driving a heat engine (in most cases, a steam turbine [9]) connected to a power cycle. Given that there is no solar radiation continuously falling upon any fixed place on earth due to its rotation movement, a backup system (energy hybridization) that burns fossil fuel (or biomass) such as Rankine and Brayton cycles is often employed.

Two configurations for the integration of a combustion chamber and a solar heater in a Brayton cycle are presented by Nathan et al. [6] (Fig. 1). The authors state that having the solar heater placed before the compressor increases the required work for compression, decreasing the global efficiency of the cycle. Spelling, in his PhD Thesis ([9]), presents two configurations for the heat components - parallel and serial positioning - as shown in Fig. 2. As stated by the author, the parallel scheme is a poor choice thermodynamically, as the inlet temperature to the turbine is below the maximum value achievable in the combustion chamber. Also, the greater the degree of utilization of solar energy in the parallel scheme, the lower the temperature entering the turbine. This makes the serial hybridisation a better choice as it can provide a final inlet temperature to the turbine that is equal to the combustor outlet temperature. Furthermore, the final temperature delivered to the turbine in the serial scheme is independent of the degree of solar integration.

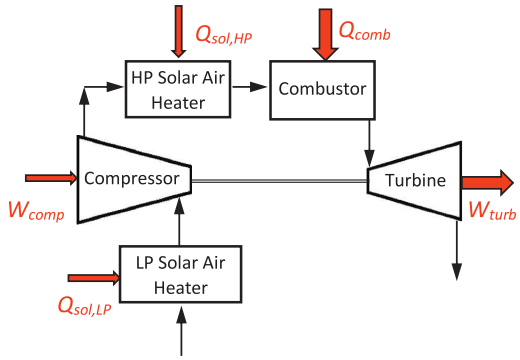

Fig. 1 Basic options to hybridise a Brayton cycle - having the solar energy source placed before the compressor ($Q_{sol,LP}$) or after ($Q_{sol,HP}$) [6].

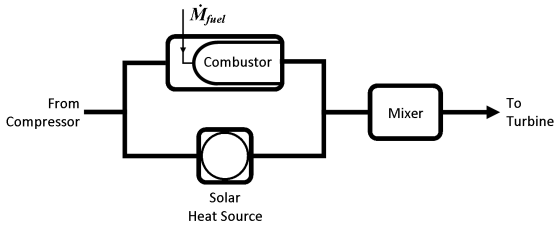

(a) Parallel configuration

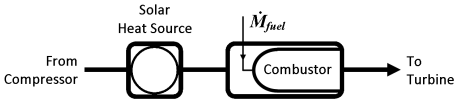

(b) In series configuration

Fig. 2 Hybridisation schemes for a gas turbine [9].

Dunham and Lipinski [2] made a thermodynamic energy analysis of the global theoretical efficiencies and power generation of a Brayton and combined Brayton-Rankine cycles with solar energy as the heat input and considering a gas microturbine. Concentration ratios characteristic of single-axis concentrator designs, such as LFC and PTC were considered. The analysis was performed for multiple selected working fluids. With a nominal solar heat input of 150 kW and a 50 kW_e gas microturbine, the single Brayton cycle reached a global efficiency of 15.31% and the combined cycle provided a 21.06% global efficiency.

The present work studies the performance of three hereby proposed thermodynamic models of combined Brayton-Rankine cycles, for different working fluids, having the previously cited work [2] as a starting point.

2. Background

A control volume is considered for each proposed model component, to which the energy balance equation presented by Shapiro et al. [5], is applied, considering steady state, and neglecting kinetic and potential energy variations. The energy rate equation is simplified to

$$\dot{Q} - \dot{W} = \iint h\,\rho(\vec{V}\cdot\vec{n})dA \tag{1}$$

The control volume can be assumed to have a series of one dimensional locations through which mass enters, i, and exits, e, the system. In this way, the surface integral in Eq. 1 can be expressed as the summation of outlet minus inlet rates of the transported variables,

$$\iint h\,\rho(\vec{V}\cdot\vec{n})dA = \sum_e \dot{m}_e\,h_e - \sum_i \dot{m}_i\,h_i$$

At steady-state the mass flow is constant and assuming uniform enthalpy at the inlet and exit sections one finally gets

$$\dot{Q} - \dot{W} = \dot{m}\left(\sum_e h_e - \sum_i h_i\right) \tag{2}$$

Different fluids are employed for the studied models, and their thermodynamic properties are accessed in each iteration throughout the computational simulations.

In the Brayton cycle, five gases are analysed - CO_2, Air, N_2, He, and H_2. The ideal gas model equations are considered to obtain the thermodynamic properties. Polynomial equations presented in equations (3a–3c) [4] are used in the implementation to provide values of specific heat, c_p, specific enthalpy, h, and specific entropy, s^0. From the specific entropy, for the ideal gas model, the value of p_r is obtained from $p_r(T) = \exp\left(s^0(T)/R\right)$.

$$c_p(T)/R = a_1T^{-2} + a_2T^{-1} + a_3 + a_4T + a_5T^2 + a_6T^3 + a_7T^4 \tag{3a}$$
$$h(T)/RT = -a_1T^{-2} + a_2\ln T/T + a_3 + a_4T/2 + a_5T^2/3 + a_6T^3/4 + a_7T^4/5 + b_1/T \tag{3b}$$
$$s^0(T)/R = -a_1T^{-2}/2 - a_2T^{-1} + a_3\ln T + a_4T + a_5T^2/2 + a_6T^3/3 + a_7T^4/4 + b_2 \tag{3c}$$

In the Rankine cycle, five other fluids are examined - R-245fa, R-141b, Cyclohexane, n-Pentane,

and Water - whose thermodynamic properties are obtained from CoolProp, which is a C++ library compatible with the software employed for the models implementation (MATLAB) that provides thermodynamic properties of a large variety of fluids.

3. Mathematical Modelling

As aforementioned, three models are proposed in this work. The models consist of combined Brayton-Rankine cycles with regeneration in the topping cycle (Brayton cycle).

The first model, schematized in Fig. 3, consists of a combined cycle fuelled by solar and combustion energy. Comparing to the combined cycle presented in the work of Dunham and Lipinski [2], model 1 differs from the former in the presence of a combustion chamber placed after the solar receiver.

In the second model, the combined cycle is fuelled by solar energy alone. It is proposed an addition of a stream bifurcation subsequent to the gas turbine in order to efficiently distribute the two resultant mass flows for the Brayton cycle and Rankine cycle, as shown in the model schematic representation in Fig. 4. In this way, the temperature of the gas after the gas turbine is preserved until it reaches the heat exchange with the bottoming cycle fluid, differently from the previous configuration in which the gas temperature decreases when passing through the regenerator before interacting with the bottoming cycle.

Model 3 implements both the new features of model 1 and model 2: an addition of a combustion chamber placed after the solar receiver and a stream splitter at the exit of the gas turbine. The schematic representation of this model can be viewed in Fig. 5.

The fixed parameters transversal to every proposed model are presented in Table 1.

The Rankine cycles fluids have fixed pressure values at the inlet of the pump, ensuring that the fluid remains either a saturated or compressed liquid at the design point of 308K. At the outlet of the pump, pressure values are fixed as well to the values presented in Table 2.

The gas is initially assumed to exit the solar receiver with a temperature, T_4, of 781 K so that h_4 is determined from the fluid's thermodynamic properties. The energy rate supplied by the receiver, $\dot{Q}_{sol}$, is, also initially, assumed to be 150 kW. In this way, the mass flow rate in the topping cycle, $\dot{m}_t$, is obtained from

$$\dot{m}_t = \frac{\dot{Q}_{sol}}{h_4 - h_3} \tag{4}$$

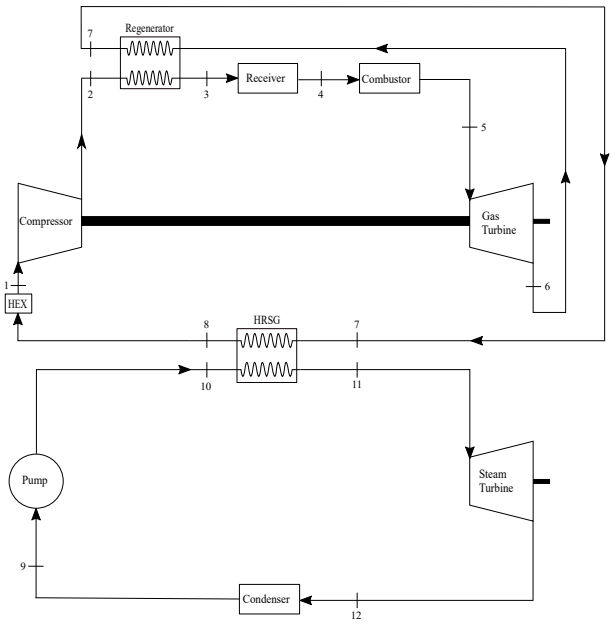

Fig. 3 Schematic presentation of Model 1.

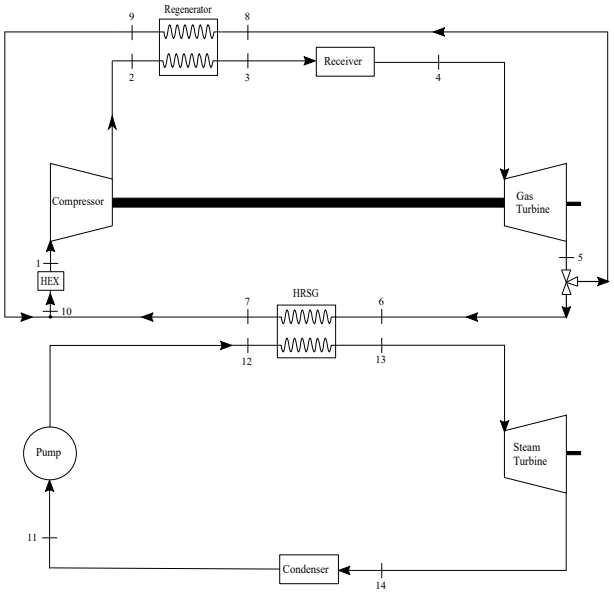

Fig. 4 Schematic presentation of Model 2.

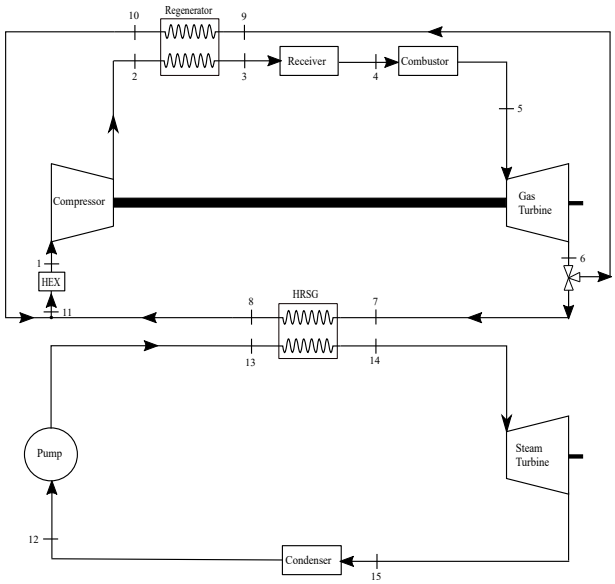

Fig. 5 Schematic presentation of Model 3.

Table 1 Fixed parameters assumed for the three models.

Cycle parameter	Design point condition
$T_{compressor\,inlet}$	308 K
$p_{compressor\,inlet}$	1 bar
C	70
$\eta_{compressor}$	79.6 %
$\eta_{gasturbine}$	85.8 %
$\eta_{steamturbine}$	68 %
$T_{pump\,inlet}$	308 K
$\Delta T_{pinch\,point}$	10 K
$T_{steam\,turbine\,inlet}$	400 K

Table 2 Assumed pressure values in the Rankine cycle.

	Pressure [bar]	
Fluid	Pump inlet	Pump outlet
R-245fa	2.109	18.75
R-141b	1.126	7.25
Cyclohexane	1	3.25
n-Pentane	1	7.25
Water	1	2.45

The efficiency at which solar heat is converted into mechanical work, is expressed as follows,

$$\eta = \underbrace{\left(\frac{\alpha C G_0 - \epsilon\sigma(T_{receiver})^4 - U_{conv}(T_{receiver} - T_{amb})}{C G_0}\right)}_{\text{Receiver efficiency}} \times \underbrace{\left(1 - \frac{T_{amb}}{T_{receiver}}\right)}_{\text{Carnot efficiency}}$$

where α is radiative absorptivity equal to 0.9, ϵ is the radiative emissivity equal to 0.2, the overall heat transfer coefficient, U_{conv}, is 10 W/m^{2}K, the standard solar irradiation, G_0, is 1 Wm^{-2}, the atmospheric temperature, $T_{amb} = 303$ K, the concentration ratio, C, is 70, and σ is the Stefan-Boltzmann constant (5.67036713×10^8 Wm^{-2}K^{-4}) [2].

Knowing that $\dot{Q}_{sol} = G_o A_{col} \eta_{receiver}$ (A_{col} is the collector area and $\eta_{receiver}$ is the efficiency of the receiver), and having at this point calculated $\dot{m}_t$ from the energy rate balance equation to the solar receiver, the following equation can be deduced,

$$G_o A_{col}\, \eta_{receiver} = \dot{m}_t\, (c_{p,4} T_4 - c_{p,3} T_3) \qquad (5)$$

In to order to obtain a corrected value of T_4, the receiver efficiency equation is substituted into the previous one. Rearranging the equation, taking into account that $T_{receiver} = T_4 + 50$ [2], a fourth degree polynomial equation of T_4 is obtained (Eq. 6), which is solved iteratively employing the *fsolve* toolbox available in MATLAB.

$$c_p T_4 = c_p T_3 + \frac{1}{\dot{m}_t} G_o A_{col} \times \left[\left(\frac{\alpha C G_0 - \epsilon\sigma(T_4 + 50)^4 - U_{conv}(T_4 + 50 - T_{amb})}{C G_0}\right)\right] \qquad (6)$$

Finally, h_4 is obtained as $h_4 = h(T_4)$, and $\dot{m}_t$ can now be corrected as well. Such proceeding is common to the three models.

In model 1, the effectiveness of the regenerator is considered to be fixed at 0.87, likewise in Dunham and Lipinki's work [2]. In the models 2 and 3, on the other hand, as it is presented the stream splitting feature, a study on the effect that the variation of the stream flows after the gas turbine has on the cycles, including on the regenerator, is performed. It is considered that these cycles' regenerator is a counterflow type of exchanger, governed by the NTU-relations (Eq. 7 [3]).

$$\epsilon_{reg} = \frac{1 - \exp[-NTU(1 - C_r)]}{1 - C_r \exp[-NTU(1 - C_r)]} \qquad (7)$$

where NTU is the number of transfer units ($NTU = UA/C_{min}$), and C_r is the heat capacity ratio ($C_r = C_{min}/C_{max} = (\dot{m}_8\, c_{p,8})/(\dot{m}_1\, c_{p,1})$) - for the case of model 2, equivalent to that of model 3.

At the Heat Recovery Steam Generator, since a phase change of the bottoming cycle fluid occurs, a pinch-point analysis is done to determine the steam mass flow, $\dot{m}_b$. The pinch point is the location where the temperature difference between the hot and cold fluids is minimum. This occurs, in this case, when the Rankine fluid is at the saturation temperature with (quality of 0%). The percentage of heat used to bring the bottoming cycle fluid from the saturated liquid state to the superheated turbine inlet state is the same as the percentage of heat used to bring the topping cycle fluid from the heat exchanger inlet state to the pinch point. This can be expressed as (for model 1's case which is equal to the others)

$$\frac{h_{11} - h_{b,pinch}}{h_{11} - h_{10}} = \frac{h_7 - h_{t,pinch}}{h_7 - h_8} \tag{8}$$

$$\dot{m}_t(h_7 - h_8) = \dot{m}_b(h_{11} - h_{10}) \tag{9}$$

The temperature at the inlet of the steam turbine is fixed at 400 K. The pressure at the inlet of the HRSG is known from Table 2. The mass flow rate at the bottoming cycle, m_b, can then be calculated from equation 9.

The net power output of the models topping cycle is the summation of the power generated by the gas turbine with the one consumed by the compressor. For instance, for model 2's subscripts, it is calculated as

$$\dot{W}_t = \dot{m}_1 \left[(h_5 - h_4) + \frac{h_1 - h_2}{\eta_{shaft}} \right] \tag{10}$$

The net power output of the bottoming cycles, similarly, is the summation of the power generated by the steam turbine with the one consumed by the pump. Considering the subscripts of model 2, it comes

$$\dot{W}_b = \dot{m}_b \Big[(h_{14} - h_{13}) + (h_{11} - h_{12}) \Big] \tag{11}$$

Regarding energy input rates, in the second model's case, the energy provided by the receiver is the only input, whilst in the other models, combustion energy rate adds to the solar. For instance, for the case of model 1, the energy input is calculated from

$$\dot{Q}_{in} = \dot{m}_1 \big[(h_4 - h_3) + (h_5 - h_4) \big] \tag{12}$$

Finally, the global efficiency values are obtained from

$$\eta_{cycle} = \frac{\dot{W}_t + \dot{W}_b}{\dot{Q}_{in}} \tag{13}$$

4. Computational Modelling

To perform the simulations and to evaluate the thermodynamic performances of the proposed models, a calculation routine was developed in MATLAB, as aforementioned.

4.1. Restrictions

The implementation of restrictions is crucial to guarantee the reliability of the results in a real life context. Those restrictions can be organized in two sets: thermodynamic properties restrictions, which are applicable across all three models; model restrictions, having some nuances that vary with the used model.

Starting with the thermodynamic properties restrictions, each working fluid in the topping and bottoming cycle of the models are constrained to operate in a certain limited temperature range. In the case of the bottoming cycle, CoolProp has these thermodynamic restrictions incorporated, preventing the program to keep running when the range values are not verified. In the Brayton cycle, however, restrictions have to be implemented given that there is no such library. These are incorporated by programming in the code so that situations such as fluid condensation do not occur.

Table 3 displays the stipulated minimum temperatures for the gases to operate in the Brayton cycles.

Table 3 Minimum temperatures for the Brayton cycle fluids.

Fluid	Lower limit temperature
CO_2	195.0 K
Air	60.0 K
N_2	63.151 K
He	2.1768 K
H_2	13.957 K

In regards to the models restrictions, the program is interrupted on situations in which a component exhibits thermal energy rate input (e.g. solar receiver) greater than that leaving the equipment (in this case, the condition $h_4 > h_3$ has to be verified). It is desired that no source of energy is needed to elevate the fluid temperature at the inlet of the compressor. In this way, the temperature at this state in all models is restricted to not go lower than 308 K. The effectiveness of the regenerator is restricted to have a maximum value of around 0.87 in order to avoid having unrealistically high values. The last

implemented restriction is to have the combustion chamber to not provide more energy than the one provided by the solar receiver ($\dot{Q}_{sol} < \dot{Q}_c$ cannot occur).

4.2. Numerical Model

In order to study the performance of the models proposed in the present work, iterations on a given span of values of pressure ratio ($p_R = p_2/p_1$) take place for different temperatures, when applied, at the exit of the combustion chamber (in the cases of model 1 and model 3). The ratio, r, between the mass flow rates resulting from the stream splitting in models 2 and 3 is assumed to have a given value.

After getting the results from these iterations, equivalent simulations are made in order to study the models behaviour with other variables, such as the mass flow ratio that governs the stream splitter after the gas turbine in models 2 and 3 and the regenerator design - heat transfer area - (models 2 and 3).

5. Results

After having the MATLAB code validated by comparing its corresponding results with those obtained by Lipinski and Dunham [2], simulations for the three models were performed.

In the subsequently presented plots, dotted lines correspond to the results without restrictions applied, whilst the solid lines refer to the results with restrictions, sometimes mentioned as acceptable results.

5.1. Model 1

Starting with model 1, as explained in the former section, a value of temperature at the inlet of the gas turbine, T_5, and a range of pressure ratio, p_R, values are chosen as input values to the program. The values of p_R are chosen to range from 1 to 20. Regarding T_5, simulations took place considering the metallurgical micro-gas turbine temperature limit, 1173 K ([1]). Results are presented in figure 6 for CO_2, chosen as the representative gas. No acceptable results for any of the fluid combinations were obtained due to the combustion chamber providing higher heat values than the solar receiver, and having temperatures at the inlet of the solar receiver to exceed those at its outlet (because the temperature values at the inlet of the regenerator hot side were disproportionally high).

Thus, temperature T_5 was lowered. The selected temperatures at state 5 were 825 K, 850 K, 875 K, and 900 K, so that the model would provide physically acceptable results. Table 4 provides the peak global cycle efficiencies obtained for model 1.

The increase of temperature T_5 yields higher values of efficiency, while also reducing the spectrum of possible results. For instance, no acceptable results

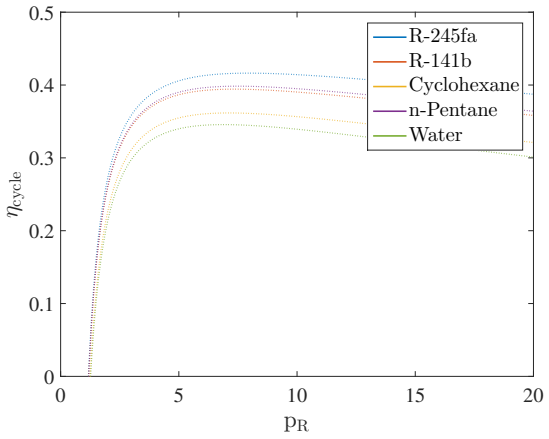

Fig. 6 Model 1: cycle global efficiency versus pressure ratio with $T_5 = 1173$ K for CO_2 and each Rankine cycle fluid.

at $T_5 = 900$ K for R-245fa were obtained (represented as "-") Thus, higher temperatures do not necessarily imply higher efficiencies. For instance, for the CO_2 and Cyclohexane case, one can observe, due to thermodynamic constraints, that the highest possible efficiency obtained with 900 K (0.1955) is lower than the highest at 875 K (0.2160). In fact, none of the results for CO_2 at $T_5 = 900$ K is better than at $T_5 = 875$ K. The highest observable value, 0.2555, corresponds to the CO_2 and n-Pentane combination at 875 K.

5.2. Model 2

The second model, containing a solar receiver as the only thermal energy source, has its temperature of the gas entering the gas turbine, T_4, calculated from the energy balance of the receiver (eq. 6) contains The range of values of the pressure ratio varies between 1 and 10, as this span covers the results of interest to the study. The regenerator effectiveness, which depends on the mass flow rates and temperatures on its cold and hot side, was calculated from the effectiveness - NTU relations.

Considering a mass flow ratio, $r = \dot{m}_8/\dot{m}_1$, and a heat transfer area of the regenerator value of 0.5 and 6 m^2, simulations with p_R as the variable input were held. For the sake of conciseness, avoiding the presentation of 25 different plots, as the global efficiency curves present the same qualitative behaviour, results are presented for the CO_2 case in fig. 7. All the efficiency curves maintain the trend of reaching a maximum value at a certain pressure ratio value.

As one can observe, the results are considerably restricted, having the global efficiency values to never reach their maximum values. Such happen due to the gas temperature restrictions, explained before. In order to reduce the magnitude of the ef-

Table 4 Peak global efficiency values for each fluid combination with T_5 = 825, 850, 875, and 900 K.

	T_5 = 825 K					T_5 = 850 K				
	CO_2	Air	N_2	He	H_2	CO_2	Air	N_2	He	H_2
R-245fa	0.2327	0.1989	0.1978	0.1550	0.1947	0.2525	0.2199	0.2189	0.1775	0.2154
R-141b	0.2189	0.1855	0.1846	0.1387	0.1820	0.2376	0.2056	0.2048	0.1605	0.2018
Cyclohexane	0.1832	0.1492	0.1484	0.0992	0.1455	0.2020	0.1695	0.1688	0.1213	0.1656
n-Pentane	0.2206	0.1870	0.1861	0.1409	0.1832	0.2395	0.2074	0.2065	0.1628	0.2033
Water	0.1703	0.1364	0.1357	0.0842	0.1328	0.1885	0.1562	0.1556	0.1063	0.1527
	T_5 = 875 K					T_5 = 900 K				
	CO_2	Air	N_2	He	H_2	CO_2	Air	N_2	He	H_2
R-245fa	-	0.2395	0.2386	0.1983	0.2347	-	-	-	-	-
R-141b	0.2527	0.2244	0.2236	0.1808	0.2203	0.2360	0.2284	0.2271	0.1931	0.2310
Cyclohexane	0.2160	0.1885	0.1879	0.1420	0.1845	0.1955	0.1898	0.1884	0.1528	0.1933
n-Pentane	0.2555	0.2263	0.2256	0.1832	0.2221	-	0.2322	0.2308	0.1968	0.2341
Water	0.2004	0.1748	0.1742	0.1269	0.1712	0.1757	0.1722	0.1708	0.1348	0.1770

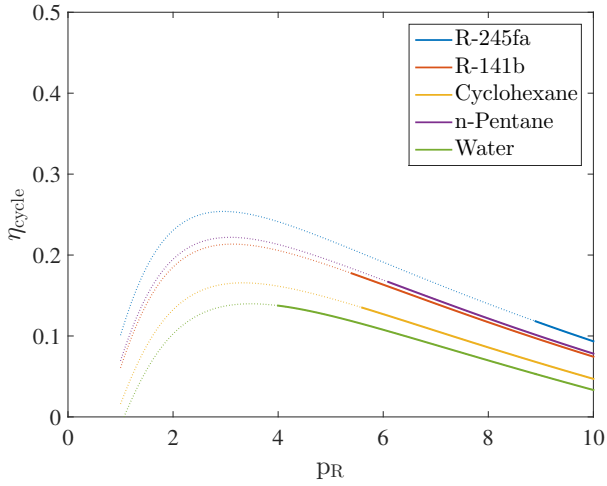

Fig. 7 Model 2: global cycle efficiency versus pressure ratio with r = 0.5 and a heat transfer area of the regenerator equal to 6 m^2 for CO_2 and each of the Rankine cycle fluids.

fect that the restrictions cause in the results, whilst pushing the curves to higher values, temperature T_{13} (steam turbine inlet) is increased. It was chosen 427 K as the maximum value since it corresponds to the lowest temperature of all the critical points of the Rankine cycle fluids. The peak global efficiency values of model 2 for T_{13} equal to 400 K and 427 K are presented in fig. 8. In general, the peak values increase, having the CO_2 and R-245fa pair case to present the most significant increase.

In order to expand the spectrum of acceptable results, the model performance was also analysed with the variation of the pinch point temperature difference, $\Delta T_{pinch\,point}$, at the HRSG. Fig. 9 show those results for the representative cases of CO_2 and R245-fa, and Air and R-141b.

As observed, the increase of the pinch point temperature difference decreases the global efficiency values, while also broadening the span of acceptable results. However, for the former fluid pair (which is the most affected by the restrictions implemented), even at the lowest efficiency curves (highest $\Delta T_{pinch\,point}$), the global cycle efficiency is higher than the value obtained with a pinch point temperature difference equal to 10 K, due to thermodynamic constraints. As it is not realistic to have $\Delta T_{pinch\,point}$ values as high as 100 K, and as it would lower every other configuration's global efficiency, its value should not differ much from the value of 10 K mentioned in the work of Dunham and Lipinski [2].

Other specification of the model cycles that influences its performance is the regenerator design and, more specifically, its heat transfer area. Thus, the behaviour of the global efficiency curves when the heat transfer area of the regenerator varies is analysed, keeping a mass flow ratio, $\dot{m}_8/\dot{m}_1$, equal to 0.5, and a temperature at the inlet of the steam turbine T_{13} = 400 K. For the sake of conciseness, the fluid pair Air and R-245fa was chosen, since the global efficiency curves show the same behaviour.

Fig. 10 shows the global efficiency evolution with the variation of the heat transfer area. The larger the regenerator heat transfer area, the greater the global cycle efficiency, since the regenerator effectiveness increases with its area of heat transfer (section 7). Furthermore, the pressure ratio at which the curves reach their maximum level tends to de-

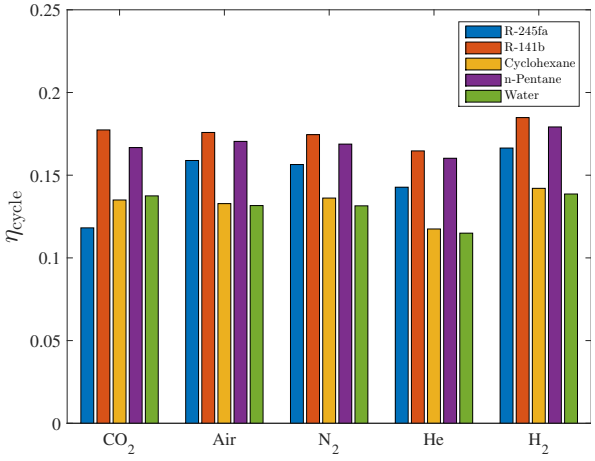

(a) 400K

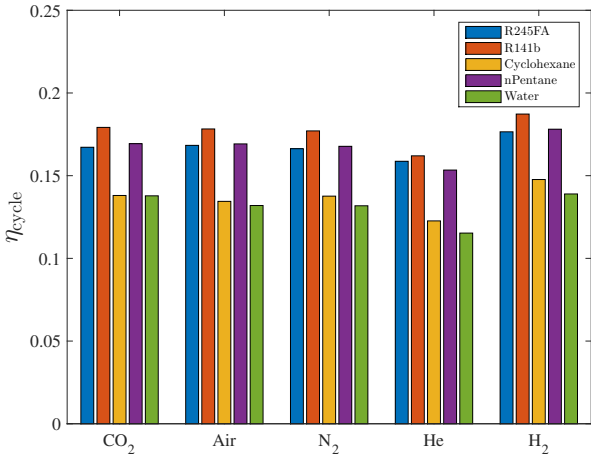

(b) 427K

Fig. 8 Model 2: global maximum efficiency values for temperatures $T_{13} = 400$ K and $T_{13} = 427$ K at the inlet of the steam turbine.

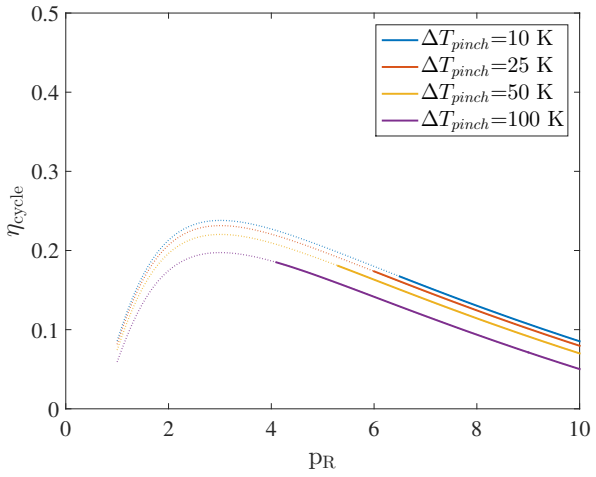

(a) CO_2 & R-245fa

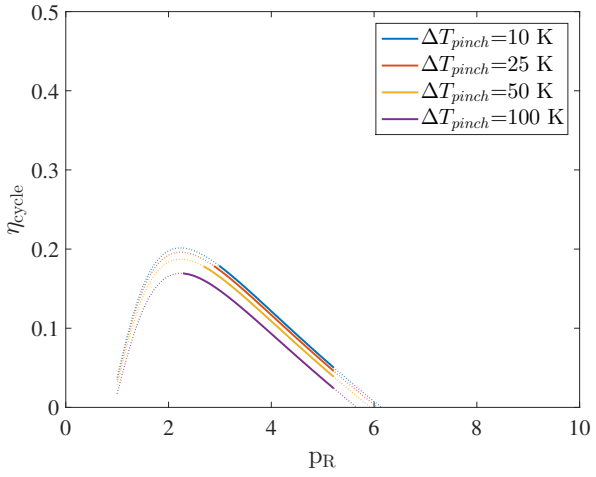

(b) Air & R-141b

Fig. 9 Model 2: global efficiency curves for different values of pinch point temperature difference with $T_{13} = 400$ K.

crease with the area increase. However, the range of physically acceptable results does not improve. It is also worth noticing that no acceptable results are obtained for areas of 8 m^2 or higher.

The mass flow ratio $r = \dot{m}_8/\dot{m}_1$ also affects the regenerator effectiveness. In the results presented in Fig. 11, the regenerator heat transfer area was kept constant and equal to 6 m^2.

The results show that the increase of the mass flow ratio implies a reduction of global efficiencies.

Nevertheless, global efficiencies greater then those of the work of Dunham and Lipinski [2] could to not be reached, which can be explained by the following reasons::

- In the mentioned authors work, the regenerator effectiveness is considered constant and equal to 0.87, whilst in the present model it depends on different parameters such as the heat transfer area, mass flow rates and specific heats, the maximum value being 0.87. This issue will be addressed in the next section.;
- This model forces the Brayton cycle fluids to go to more extreme conditions due to its own configuration by having the stream bifurcation, which implies more severe restrictions in the operating conditions.

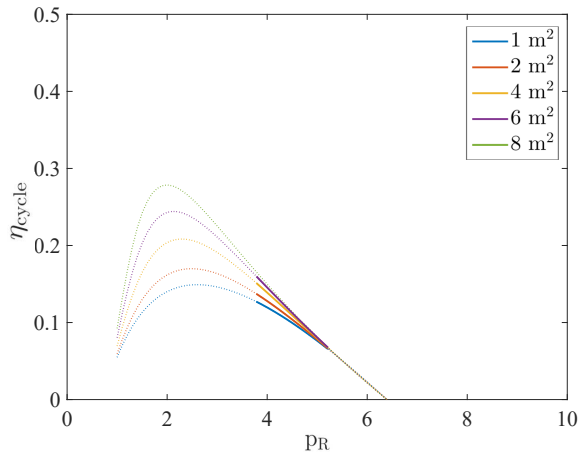

Fig. 10 Model 2: regenerator heat transfer area influence on global cycle efficiency, for the fluid pair Air and R-245fa, assuming T_{13} = 400 K, $\Delta T_{pinch\,point}$ = 10 K and a mass flow ratio $r = \dot{m}_8/\dot{m}_1 = 0.5$.

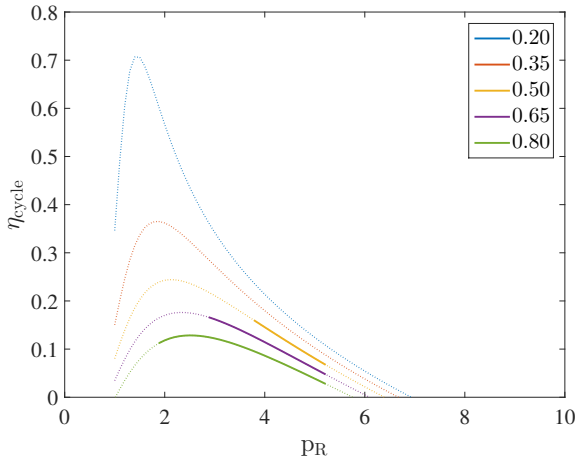

Fig. 11 Model 2: mass flow ratio $r = \dot{m}_8/\dot{m}_1$ influence on global cycle efficiency, for the fluid pair Air and R-245fa, assuming a regenerator heat transfer area equal to 6 m^2, T_{13}=400 K and $\Delta_{pinch\,point}$ = 10 K.

5.3. Model 3

Similarly to the first model situation, no acceptable results for T_5 = 1173 K were obtained due to the applied restrictions. Fig 12 shows the results obtained for CO_2 and each of the Rankine cycle fluids.

However, when compared to the peak efficiencies in model 1, using the same temperature T_5 = 1173 K (Fig. 6), the global efficiencies of model 3 are considerably lower. Such outcome is mainly due to the fact that in model 1 (as well as in the work of Dunham and Lipinski [2]) the regenerator effectiveness was considered constant and equal to 0.87, whereas in models 2 and 3 this parameter was calculated using the NTU relations, imposing a maximum value of 0.87. To make a comparison on equal terms, the same procedure should be applied to model 1. Results for CO_2 as the representative gas are presented in Fig. 13 (model 1) and Fig. 14 (model 3), assuming a temperature at the inlet of the gas turbine T_5 = 825 K and a regenerator heat transfer area of 6 m^2.

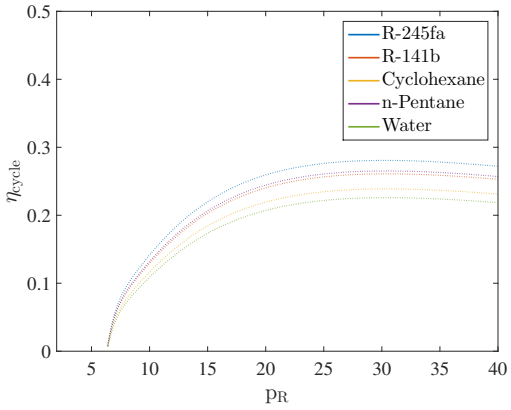

Fig. 12 Model 3: global cycle efficiency assuming T_5 = 1173 K, a regenerator heat transfer area equal to 6 m^2 and a mass flow ratio r = 0.5.

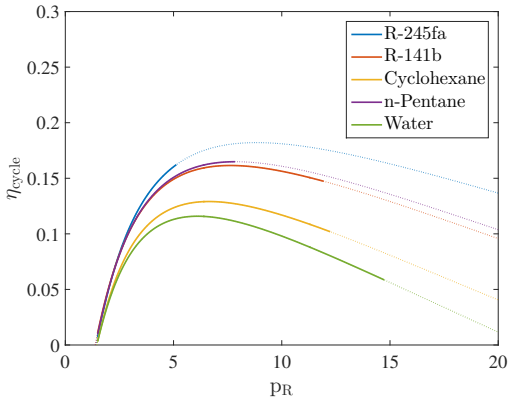

Fig. 13 Model 1: global cycle efficiency assuming T_5 = 825 K and a regenerator heat transfer area equal to 6 m^2 for CO_2 and each Rankine cycle fluid.

The results show that model 3 outperforms model 1. With the exception of the pair CO_2 and R-245fa, every fluid combination in model 3 yields higher peak global efficiencies than in the case of model 1, demonstrating that the stream splitting feature improves the global cycle efficiencies.

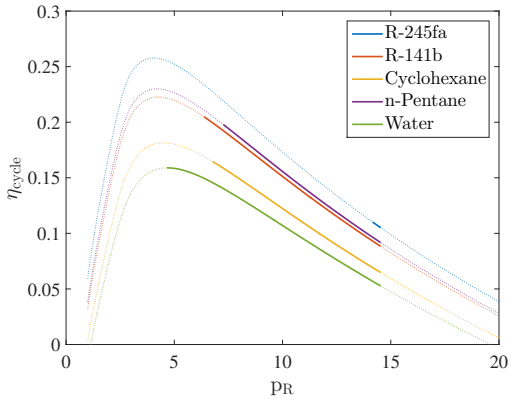

Fig. 14 Model 3: global cycle efficiency assuming $T_5 = 825$ K, a regenerator heat transfer area equal to 6 m^2 and a mass flow ratio $r = 0.5$ for CO_2 and each Rankine cycle fluid.

6. Conclusions

The main goal of this work was to study the performance of three combined Brayton-Rankine cycles with solar thermal power generation and, if possible, improve the results of the work of Dunham and Lipinski [2].

In retrospect, some final considerations can be drawn. With the model operating with the same Brayton cycle regenerator design conditions, as in the work of Dunham and Lipinski [2] ($\epsilon_{reg} = 0.87$), having a combustion chamber supporting the solar receiver in the generation of heat (with $\dot{Q}_c < \dot{Q}_{sol}$) provides higher global efficiencies than with solar alone. This also supports the idea that the combination of both types of energy can feed a power cycle more efficiently.

With ϵ_{reg} being obtained from the NTU-effectiveness relations, models 2 and 3 outperform model 1, which is similar to the cycle studied in the work of Dunham and Lipinski [2]. Such results allow us to conclude that the implementation of the stream splitter is beneficial.

The fluid pair CO_2 and R-245fa provides the highest global cycle efficiency for all the models. In the case of model 2 and 3, however, due to the stream splitting, this pair is the most affected in terms of thermodynamic restrictions, resulting in the lowest global efficiencies, despite having better maximum efficiencies.

References

[1] L. Aichmayer, J. Spelling, and B. Laumert. Preliminary design and analysis of a novel solar receiver for a micro gas-turbine based solar dish system. *Solar Energy*, 114:378–396, 2015.

[2] M. T. Dunham and W. Lipiński. Thermodynamic Analyses of Single Brayton and Combined Brayton–Rankine Cycles for Distributed Solar Thermal Power Generation. *Journal of Solar Energy Engineering*, 135(3):031008, 2013.

[3] F. P. Incropera, T. L. Bergman, A. S. Lavine, and D. P. DeWitt. *Fundamentals of Heat and Mass Transfer*. 2011.

[4] B. J. Mcbride, M. J. Zehe, and S. Gordon. NASA Glenn Coefficients for Calculating Thermodynamic Properties of Individual Species. September, 2002.

[5] M. Moran J. *Fundamentals Of Engineering Thermodynamics*. Number 9. 7th edition, 2013.

[6] G. J. Nathan, M. Jafarian, B. B. Dally, W. L. Saw, P. J. Ashman, E. Hu, and A. Steinfeld. Solar thermal hybrids for combustion power plant: A growing opportunity. *Progress in Energy and Combustion Science*, 64:4–28, 2018.

[7] E. Pihl, J. Spelling, and F. Johnsson. Thermo-Economic Optimization of Hybridization Options for Solar Retrofitting of Combined-Cycle Power Plants. *Journal of Solar Energy Engineering*, 136(2):021001, 2013.

[8] SolarPACES. https://www.solarpaces.org/csp-technologies/csp-projects-around-the-world/, 2019.

[9] J. Spelling. *Hybrid Solar Gas-Turbine Power Plants - A Thermoeconomic Analysis*. PhD thesis, 2013.

[10] H. L. Zhang, J. Baeyens, J. Degrève, and G. Cacères. Concentrated solar power plants: Review and design methodology. *Renewable and Sustainable Energy Reviews*, 22:466–481, 2013.